Three-band non-Hermitian non-Abelian topological insulator with $\mathcal{PT}$ symmetry

Yanmeng Liang,[1] Rui Wang,[1] Zhizhou Yu,[2,*] Jun Chen,[3,4] Liantuan Xiao,[1,4] Suotang Jia,[1,4] and Lei Zhang[1,4,†]

[1]*State Key Laboratory of Quantum Optics and Quantum Optics Devices, Institute of Laser Spectroscopy, Shanxi University, Taiyuan 030006, China*

[2]*School of Physics and Technology, Nanjing Normal University, Nanjing 210023, China*

[3]*State Key Laboratory of Quantum Optics and Quantum Optics Devices, Institute of Theoretical Physics, Shanxi University, Taiyuan 030006, China*

[4]*Collaborative Innovation Center of Extreme Optics, Shanxi University, Taiyuan 030006, China*

(Received 23 November 2023; revised 23 January 2024; accepted 28 February 2024; published 14 March 2024)

Non-Abelian topological charges have recently been proposed to characterize the noncommutative topological properties in multiple-band-gap systems. In this work, we investigate a non-Abelian system based on a three-band tight-binding model characterized by quaternions. By introducing nonreciprocal hopping, the system becomes non-Hermitian yet still preserves $\mathcal{PT}$ symmetry within a range of hopping parameters. As the hopping strength increases, the $\mathcal{PT}$ symmetry is spontaneously broken. We find that the critical hopping values of $\mathcal{PT}$ transitions for quaternion charges $\{\pm i, \pm k, -1\}$ are different from that of the $\pm j$ case. Non-Hermitian quaternion topological charges are analytically analyzed using the Berry-Wilczek-Zee (BWZ) phase. By diagonalizing the BWZ phase matrix, we discover that its eigenvalues undergo a real-to-imaginary $\mathcal{PT}$ transition. This corresponds to the real-to-imaginary transition of the associated eigenvalues of the Hamiltonian. However, the boundary states in the finite system remain robust against random disorder only when the $\mathcal{PT}$ symmetry is preserved. Furthermore, we examine the existence of domain wall states between two subsystems carrying different topological charges to verify the non-Abelian quotient relation in the non-Hermitian situation. It is revealed that domain wall states are no longer robust against random disorder once the $\mathcal{PT}$ symmetry is broken. Our work deepens the physical understanding of the non-Abelian topology in the non-Hermitian system with $\mathcal{PT}$ symmetry.

DOI: 10.1103/PhysRevB.109.115127

I. INTRODUCTION

Recently, the exploration of non-Abelian topological physics has received significant attention both theoretically and experimentally [1–8]. To date, many experiments have been conducted in various physical systems to confirm the non-Abelian topology, including photonic systems [2,9], phononic systems [10,11], and transmission lines [4,12]. Non-Abelian groups have played a crucial role in characterizing topological properties of nodal line semimetals in three dimensions [1–3,6,10,13] and boundary states in three-band models [4] and four-band models [12]. Non-Abelian topological charges can be protected by the system's combined $\mathcal{PT}$ symmetry, exhibiting robustness against perturbations and even random disorders. Here, $\mathcal{PT}$-symmetric systems are those that remain unchanged under the combined operations of parity ($\mathcal{P}$) and time-reversal ($\mathcal{T}$) symmetry.

On the other hand, non-Hermitian topological physics has garnered significant attention [5,14–22]. Non-Hermiticity is typically achieved through the introduction of nonreciprocal hopping terms or non-Hermitian gain and loss terms. Non-Hermitian systems exhibit a plethora of intriguing phenomena, including the non-Hermitian skin effect [22–27], broken bulk-boundary correspondence [28–33], complex eigenspectra, complex energy gaps, and exceptional points [15,34–39], among others. In non-Hermitian systems, eigenvalues and eigenfunctions are generally complex. However, if non-Hermitian Hamiltonians possess $\mathcal{PT}$ symmetry, they can exhibit a purely real eigenvalue spectrum within a range of parameters [18,40,41]. Spontaneous $\mathcal{PT}$-symmetry breaking transitions between real and complex eigenvalues occur, leading to complex eigenvalues and eigenfunctions. Such spontaneous $\mathcal{PT}$-symmetry breaking typically manifests at an exceptional point (EP). EPs refer to points in the parameter space of a system where two or more eigenvalues and their corresponding eigenvectors coalesce or merge into a single entity. In non-Hermitian systems, EPs are commonly associated with topological charge and geometric (Berry) phase [42,43]. Consequently, extensive research has been conducted on various $\mathcal{PT}$-symmetric systems, including the Anderson models for disorder systems [44,45], the Dirac Hamiltonians of topological insulators [46], and open quantum systems [47]. Moreover, considerable attention has been given to studying non-Hermitian $\mathcal{PT}$-symmetric discrete systems, such as the tight-binding chain [5,48]. However, the non-Hermitian non-Abelian topological systems are less studied.

Based on the non-Abelian three-band tight-binding model, we introduce the nonreciprocal hopping strength γ into the system. We analytically obtain the energy spectrum versus the hopping parameter. It is found that the $\mathcal{PT}$ symmetry is preserved until γ reaches the critical points. The critical hopping values of $\mathcal{PT}$ transitions for quaternion charges $\{\pm i, \pm k, -1\}$

*yuzhizhou@njnu.edu.cn
†zhanglei@sxu.edu.cn

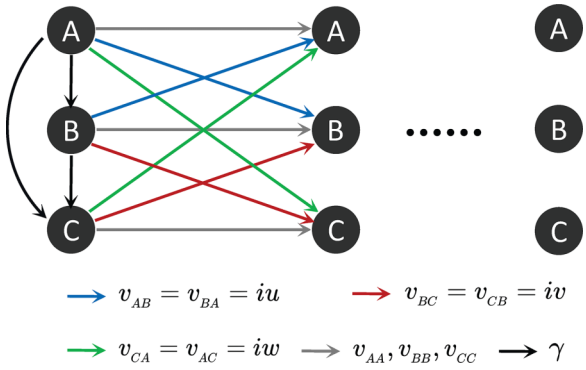

FIG. 1. Schematic plot of the tight-binding model with nearest-neighbor hoppings; each unit cell consists of three meta-atoms A, B, and C. The nearest-neighbor hopping strengths are defined as $v_{AB} = v_{BA} = iu$ (blue), $v_{CA} = v_{AC} = iw$ (green), and $v_{BC} = v_{CB} = iv$ (red). The nonreciprocal hopping strength is denoted by γ.

are different from that of the $\pm j$ case. The topological charges are analytically computed by the Berry-Wilczek-Zee (BWZ) phase matrix. The eigenvalues of the BWZ phase matrix also undergo a real-to-imaginary $\mathcal{PT}$ transition, which corresponds to the real-to-imaginary transition of the associated eigenvalues of the Hamiltonian. More importantly, the boundary states in the finite system remain robust against random disorder introduced in the on-sites only when the $\mathcal{PT}$ symmetry is preserved. To investigate the non-Abelian quotient relation, we consider the domain wall states in two different scenarios, i.e., one Hermitian and non-Hermitian subsystems and two non-Hermitian subsystems. By connecting two subsystems carrying different topological charges, the domain wall states always emerge. It is also found that domain states are no longer robust against random disorder when $\mathcal{PT}$ symmetry is broken.

This paper is structured as follows. In Sec. II, we demonstrate a non-Hermitian non-Abelian three-band tight-binding model. In Sec. III, we analytically calculate the eigenvalues, eigen-wave-functions, and non-Hermitian non-Abelian topological charges via BWZ phase matrix. Additionally, we investigate the effect of random disorder on the boundary states and domain wall states when the nonreciprocal hopping γ is present. Finally, a brief summary is given in Sec. IV.

II. NON-HERMITIAN NON-ABELIAN THREE-BAND TIGHT-BINDING MODEL

As shown in Fig. 1, we consider a three-band tight-binding model in a quasi-one-dimensional lattice with the nearest-neighbor (NN) and next-nearest-neighbor (NNN) hoppings, which can be classified by the quaternion group $\mathbb{Q} = (+1, \pm i, \pm j, \pm k, -1)$. There are three inequivalent lattice sites in each unit cell, labeled separately as A, B, and C. Starting from the tight-binding Hamiltonian [4]

$$\mathcal{H}_0 = \sum_n \left(\sum_{X=A,B,C} s_{XX} c^\dagger_{X,n} c_{X,n} + \sum_{\substack{X=A,B,C \\ Y=A,B,C}} v_{XY} c^\dagger_{X,n} c_{Y,n+1} + \sum_{\substack{X=A,B,C \\ Y=A,B,C}} v_{XYl} c^\dagger_{X,n} c_{Y,n+2} + \text{H.c.} \right), \tag{1}$$

where the first term in $\mathcal{H}_0$ represents the on-site energy, the second term represents NN hoppings, and the last term represents NNN hoppings. The $c^\dagger_{X,n}$ and $c_{X,n}$ denote the creation and annihilation operators on the sublattice X/Y and site n, respectively. The s_{XX} is the on-site energy parameter, v_{XY} is the nearest-neighbor hopping parameter, and v_{XYl} is the next-nearest-neighbor hopping parameter. It is important to note that for non-Abelian topological charges $\pm i$, $\pm j$, $\pm k$, we only consider NN hoppings. Conversely, for non-Abelian topological charge -1, we only consider the NNN hoppings. Based on Eq. (1), we incorporate the non-Hermitian part $\mathcal{H}^{(Q)}_\gamma$ into the system,

$$\mathcal{H}^{(Q)} = \mathcal{H}_0 + \mathcal{H}^{(Q)}_\gamma. \tag{2}$$

For the topological $Q = \pm i$ case, the nonreciprocal hopping is introduced between the B and C atoms in Fig. 1. $\mathcal{H}^{(Q)}_\gamma$ equals

$$\mathcal{H}^{(i)}_\gamma = \gamma \sum_n (c^\dagger_{B,n} c_{C,n} - c^\dagger_{C,n} c_{B,n}). \tag{3}$$

For the topological $Q = \pm j$ case, the nonreciprocal hopping is introduced between the A and C atoms in Fig. 1. $\mathcal{H}^{(Q)}_\gamma$ equals

$$\mathcal{H}^{(j)}_\gamma = \gamma \sum_n (c^\dagger_{A,n} c_{C,n} - c^\dagger_{C,n} c_{A,n}). \tag{4}$$

For the topological $Q = \pm k$ and $Q = -1$ cases, the nonreciprocal hopping is introduced between the A and B atoms in Fig. 1. $\mathcal{H}^{(Q)}_\gamma$ equals

$$\mathcal{H}^{(k/-1)}_\gamma = \gamma \sum_n (c^\dagger_{A,n} c_{B,n} - c^\dagger_{B,n} c_{A,n}). \tag{5}$$

Once the nonreciprocal hoppings denoted as γ become nonzero, the system transitions to a non-Hermitian state.

After the Fourier transformation, the Hamiltonian is represented in k space for different topological charges,

$$H_0^{(i/j/k)}(k) = \begin{bmatrix} s_{AA} + 2v_{AA}\cos k & 2u\sin k & 2w\sin k \\ 2u\sin k & s_{BB} + 2v_{BB}\cos k & 2v\sin k \\ 2w\sin k & 2v\sin k & s_{CC} + 2v_{CC}\cos k \end{bmatrix}, \tag{6}$$

$$H_0^{(-1)}(k) = \begin{bmatrix} s_{AA} + 2v_{AAl}\cos 2k & 2u_l\sin 2k & 2w_l\sin 2k \\ 2u_l\sin 2k & s_{BB} + 2v_{BBl}\cos 2k & 2v_l\sin 2k \\ 2w_l\sin 2k & 2v_l\sin 2k & s_{CC} + 2v_{CCl}\cos 2k \end{bmatrix}, \tag{7}$$

$$H^{(Q)}(k) = H_0^{(Q)}(k) + \gamma(-1)^{l-1} \sum_{mn} \epsilon_{lmn} |m\rangle\langle n|, \tag{8}$$

TABLE I. Parameters of various non-Abelian topological charges Q in the ideal tight-binding model for the Hermitian case.

Q	s_{AA}	s_{BB}	s_{CC}	v_{AA}	v_{BB}	v_{CC}	u	v	w
$+i$	1	5/2	5/2	0	1/4	−1/4	0	1/4	0
$-i$	1	5/2	5/2	0	1/4	−1/4	0	−1/4	0
$+j$	2	2	2	1/2	0	−1/2	0	0	−1/2
$-j$	2	2	2	1/2	0	−1/2	0	0	1/2
$+k$	3/2	3/2	3	1/4	−1/4	0	1/4	0	0
$-k$	3/2	3/2	3	1/4	−1/4	0	−1/4	0	0
Q	s_{AA}	s_{BB}	s_{CC}	v_{AAl}	v_{BBl}	v_{CCl}	u_l	v_l	w_l
−1	3/2	3/2	3	−1/4	1/4	0	−1/4	0	0

where for the $Q = i$ case, $l = 1$; for the $Q = j$ case, $l = 2$; for the $Q = k, -1$ cases, $l = 3$; ϵ_{lmn} is a three-dimensional Levi-Civita symbol; and $m, n \in \{1, 2, 3\}$, $|1\rangle = (1, 0, 0)^T$, $|2\rangle = (0, 1, 0)^T$, $|3\rangle = (0, 0, 1)^T$. We have set $v_{AB} = v_{BA} = iu$, $v_{ABl} = v_{BAl} = iu_l$, $v_{CA} = v_{AC} = iw$, $v_{CAl} = v_{ACl} = iw_l$ and $v_{BC} = v_{CB} = iv$, $v_{BCl} = v_{CBl} = iv_l$ to make the Bloch Hamiltonian explicitly real (u, u_l, v, v_l, w, w_l are all real). The parameters for various topological charges in the Hermitian case ($\gamma = 0$) are summarized in Table I.

Before exploring the effects of introducing nonreciprocal hopping into the non-Abelian system, we study $\mathcal{PT}$ symmetry property of non-Hermitian non-Abelian system by defining the parity operator $\mathcal{P}^{(Q)}$. Its action satisfies $(\mathcal{P}^{(Q)})^{-1} H_0^{(Q)}(k) \mathcal{P}^{(Q)} = H_0^{(Q)}(-k)$. The parity operators $\mathcal{P}^{(Q)}$ are

$$\mathcal{P}^{(i/j)} = \begin{bmatrix} 1 & 0 & 0 \\ 0 & 1 & 0 \\ 0 & 0 & -1 \end{bmatrix}, \quad \mathcal{P}^{(k/-1)} = \begin{bmatrix} 1 & 0 & 0 \\ 0 & -1 & 0 \\ 0 & 0 & 1 \end{bmatrix}. \quad (9)$$

Correspondingly, the time-reversal operators $\mathcal{T}^{(Q)}$ can be expressed as

$$\mathcal{T}^{(i/j)} = \begin{bmatrix} 1 & 0 & 0 \\ 0 & 1 & 0 \\ 0 & 0 & -1 \end{bmatrix} \mathcal{K}, \quad \mathcal{T}^{(k/-1)} = \begin{bmatrix} 1 & 0 & 0 \\ 0 & -1 & 0 \\ 0 & 0 & 1 \end{bmatrix} \mathcal{K}, \quad (10)$$

where $\mathcal{K}$ is the complex-conjugation operator. We can find that $(\mathcal{T}^{(Q)})^{-1} H_0^{(Q)}(k) \mathcal{T}^{(Q)} = H_0^{(Q)*}(-k)$. So $H_0^{(Q)}(k)$ has $\mathcal{PT}$ symmetry $(\mathcal{P}^{(Q)}\mathcal{T}^{(Q)})^{-1} H_0^{(Q)}(k) (\mathcal{P}^{(Q)}\mathcal{T}^{(Q)}) = H_0^{(Q)*}(k)$ with $\mathcal{P}^{(Q)}\mathcal{T}^{(Q)} = \mathcal{K}$. Furthermore, we can verify that the non-Hermitian part $H_\gamma^{(Q)}(k) = \gamma(-1)^{l-1} \sum_{mn} \epsilon_{lmn} |m\rangle\langle n|$ also maintains $\mathcal{PT}$ symmetry.

III. RESULTS AND DISCUSSION

A. Eigenvalues and $\mathcal{PT}$ symmetry breaking

By incorporating nonreciprocal hoppings, denoted as γ, into the Hamiltonian shown in Eq. (2), the $\mathcal{PT}$ symmetry is preserved until γ reaches a critical value. Hence, the

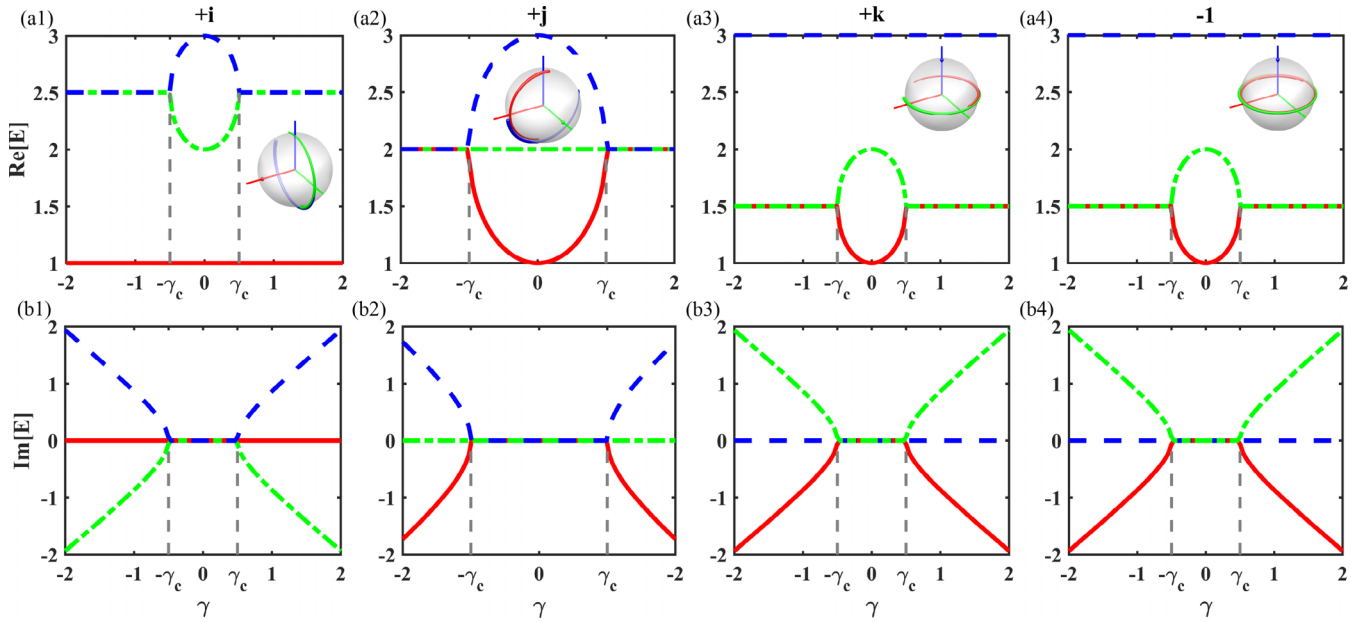

FIG. 2. The real parts (a1)–(a4) and imaginary parts (b1)–(b4) of bulk-band energy versus γ for different non-Abelian topological charges $+i$, $+j$, $+k$, and -1 in non-Hermitian cases. The insets in panels (a1)–(a4) display the corresponding eigenstate frame spheres when $\gamma = 0.3$. Critical points $\pm\gamma_c$ are indicated by dotted gray lines.

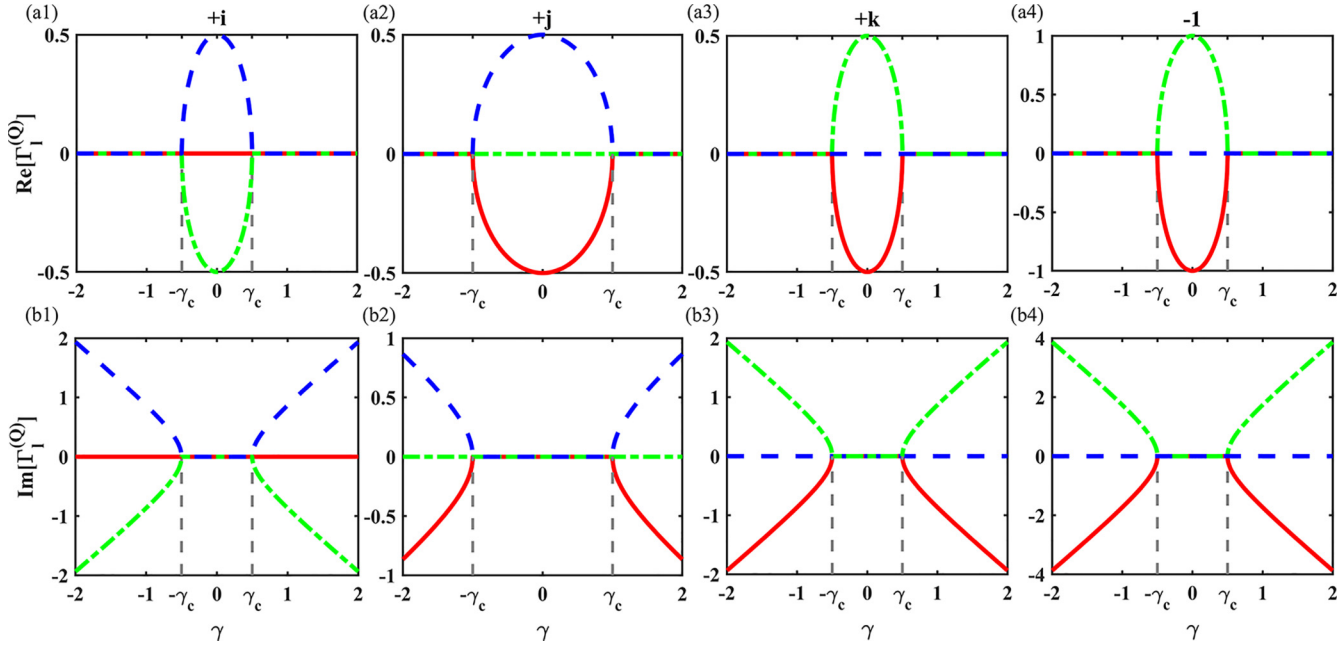

FIG. 3. The real parts (a1)–(a4) and imaginary parts (b1)–(b4) of BWZ phase matrices' eigenvalues $\Gamma_l^{(Q)}$ with $l = 1, 2, 3$ versus γ for different non-Abelian topological charges $+i$, $+j$, $+k$, and -1 in non-Hermitian cases. Critical points $\pm\gamma_c$ are indicated by dotted gray lines.

corresponding eigenvalues are real-valued for any wave vector k in the Brillouin zone when γ is small. The eigenvalues corresponding to the Hamiltonian in Eq. (8) can be found by diagonalization:

$$E_1^{(+i)} = 1, \quad E_{2,3}^{(+i)} = \frac{5}{2} \mp \frac{\sqrt{1-4\gamma^2}}{2}, \tag{11}$$

$$E_2^{(+j)} = 2, \quad E_{1,3}^{(+j)} = 2 \mp \sqrt{1-\gamma^2}, \tag{12}$$

$$E_3^{(+k/-1)} = 3, \quad E_{1,2}^{(+k/-1)} = \frac{3}{2} \mp \frac{\sqrt{1-4\gamma^2}}{2}. \tag{13}$$

Here, $E_i^{(Q)}$ represents the eigenvalue, with the subscript i ($i = 1, 2, 3$) indicating the ith band and the superscript Q representing non-Abelian topological charges $+i$, $+j$, $+k$, and -1 in the Hermitian case. It is worth noting that all bands are flat in k space. Since $-i$, $-j$, and $-k$ correspond to conjugate elements with inverse rotations, we will focus on the $+i$, $+j$, and $+k$ cases in the following discussion. It is observed that when $\gamma = 0$, all these eigenvalues are real. However, by introducing a small γ, all bulk band energies remain purely real for $|\gamma| \leqslant \gamma_c$ as depicted in Fig. 2. When the magnitude of γ exceeds a critical value, known as the exceptional point γ_c, the bulk band energies become complex, and the $\mathcal{PT}$ symmetry is spontaneously broken. According to Eqs. (11)–(13), the critical value $\gamma_c = 0.5$ applies for the $Q = +i, +k, -1$ cases, but 1 for the $Q = +j$ case. Figures 2(a1) and 2(b1) illustrate that the real parts of the second and third bulk bands merge at critical points $\pm\gamma_c$ while the corresponding imaginary parts become nonzero after these points for the $Q = +i$ case. In the $Q = +k, -1$ cases, the real parts of the first and second bands merge without any distinction from the band structure perspective. It is also found that the real parts of the first and third bulk bands merge at critical points $\gamma_c = 1$ for the $Q = +j$ case.

B. Non-Abelian topological charges in non-Hermitian cases

To characterize the topological property of the non-Hermitian non-Abelian system, we first introduce the non-Hermitian non-Abelian Berry connection, also known as the non-Abelian Berry-Wilczek-Zee (BWZ) connection [5,49,50],

$$A_{\alpha\beta}^{(Q)}(k) = i\langle\phi_\alpha^{(Q)}|\partial_k|\psi_\beta^{(Q)}\rangle, \tag{14}$$

where $\alpha, \beta = 1, 2, 3$. The eigen-wave-functions $|\psi_\alpha^{(Q)}\rangle$ and $|\phi_\alpha^{(Q)}\rangle$ can be obtained,

$$H^{(Q)}|\psi_\alpha^{(Q)}\rangle = E_\alpha^{(Q)}|\psi_\alpha^{(Q)}\rangle \tag{15}$$

and

$$(H^{(Q)})^\dagger|\phi_\alpha^{(Q)}\rangle = \left(E_\alpha^{(Q)}\right)^*|\phi_\alpha^{(Q)}\rangle. \tag{16}$$

Then the non-Abelian BWZ phase matrix element can be obtained to characterize the topological property of the proposed Hamiltonian in Eq. (2),

$$\Gamma_{\alpha\beta}^{(Q)} = \frac{1}{2\pi}\int_0^{2\pi} A_{\alpha\beta}^{(Q)}(k)dk. \tag{17}$$

As an illustration, the eigen-wave-functions corresponding to $Q = +i$ are analytically solved as

$$|\psi_1^{(+i)}\rangle = \{1, 0, 0\}, \tag{18}$$

$$|\psi_{2,3}^{(+i)}\rangle = \{0, (\cos k \mp \sqrt{1-4\gamma^2})/(\sin k - 2\gamma), 1\}, \tag{19}$$

$$|\phi_1^{(+i)}\rangle = \{1, 0, 0\}, \tag{20}$$

$$|\phi_{2,3}^{(+i)}\rangle = \{0, (\cos k \mp \sqrt{1-4\gamma^2})/(\sin k + 2\gamma), 1\}. \tag{21}$$

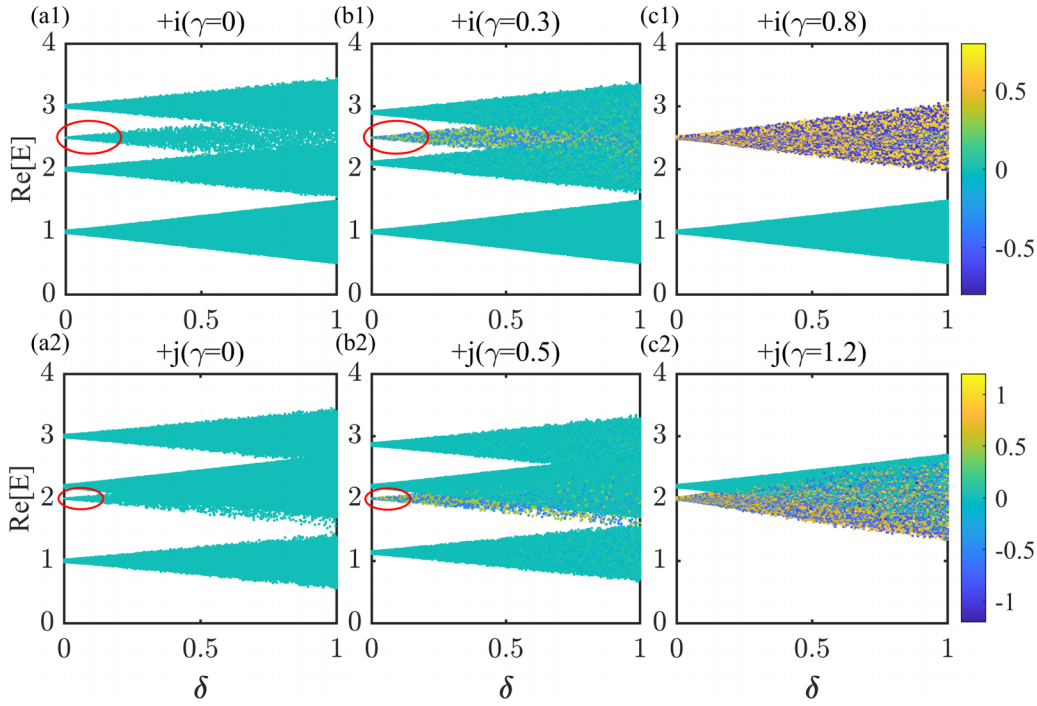

FIG. 4. (a1)–(c1) The real parts of energy spectrum vs the disorder strength δ with different nonreciprocal hopping strengths $\gamma = 0$, $\gamma = 0.3$, and $\gamma = 0.8$ for topological charge $+i$ case. (a2)–(c2) The real parts of energy spectrum vs the disorder strength δ with different nonreciprocal hopping strengths $\gamma = 0$, $\gamma = 0.5$, and $\gamma = 1.2$ for topological charge $+j$ case. Here $s_{BB} = 2.2$ for charge $+j$; other parameters are the same as those in Table I. The color bar corresponds to the imaginary parts of the energy spectrum. The red ellipses indicate the corresponding edge states. Here 21 unit cells are used in the numerical calculation; 10 configurations are calculated for each disorder strength δ.

The eigen-wave-functions for other cases can be found in the Appendix. In the inset of Figs. 2(a1)–2(a4), the rotations of the eigenstate ($|\psi_\alpha^{(Q)}\rangle$) frames are plotted when $\gamma = 0.3$. For the $Q = +i$ case, the eigenstate of the first band remains unchanged, while the eigenstates of the second and third bands rotate through π when k ranges from $-\pi$ to π. For $Q = +j$, the eigenstate of the second band remains unchanged, while the eigenstates of the first and third bands rotate by π. Similarly, for the $Q = +k, -1$ cases, the eigenstate of the third band remains unchanged, and the eigenstates of the first and second bands rotate by π and 2π, respectively. Note that when $\mathcal{PT}$ symmetry is broken, the wave function becomes complex and the eigenstate frame is no longer well defined.

When there is no nonreciprocal hopping, i.e., $\gamma = 0$, we analytically calculate the non-Abelian BWZ connection by Eq. (14) and hence the non-Abelian BWZ phase matrices

$$\Gamma^{(+i)} = \begin{pmatrix} 0 & 0 & 0 \\ 0 & 0 & \frac{i}{2} \\ 0 & -\frac{i}{2} & 0 \end{pmatrix}, \quad \Gamma^{(+j)} = \begin{pmatrix} 0 & 0 & \frac{i}{2} \\ 0 & 0 & 0 \\ -\frac{i}{2} & 0 & 0 \end{pmatrix},$$
$$\Gamma^{(+k)} = \begin{pmatrix} 0 & \frac{i}{2} & 0 \\ -\frac{i}{2} & 0 & 0 \\ 0 & 0 & 0 \end{pmatrix}, \quad \Gamma^{(-1)} = \begin{pmatrix} 0 & -i & 0 \\ i & 0 & 0 \\ 0 & 0 & 0 \end{pmatrix}. \quad (22)$$

Note that the non-Abelian BWZ phase matrices vary with different non-Abelian topological charges.

Similarly, the non-Hermitian non-Abelian BWZ phase matrices can also be analytically obtained,

$$\Gamma^{(+i)} = \begin{pmatrix} 0 & 0 & 0 \\ 0 & -i\gamma & \frac{i}{2} \\ 0 & -\frac{i}{2} & i\gamma \end{pmatrix}, \quad \Gamma^{(+j)} = \begin{pmatrix} \frac{i\gamma}{2} & 0 & \frac{i}{2} \\ 0 & 0 & 0 \\ -\frac{i}{2} & 0 & -\frac{i\gamma}{2} \end{pmatrix},$$
$$\Gamma^{(+k)} = \begin{pmatrix} -i\gamma & \frac{i}{2} & 0 \\ -\frac{i}{2} & i\gamma & 0 \\ 0 & 0 & 0 \end{pmatrix}, \quad \Gamma^{(-1)} = \begin{pmatrix} -2i\gamma & -i & 0 \\ i & 2i\gamma & 0 \\ 0 & 0 & 0 \end{pmatrix}. \quad (23)$$

Through the analytical diagonalization of the non-Abelian BWZ phase matrices, we discover that their eigenvalues undergo a real-to-imaginary $\mathcal{PT}$ transition. This corresponds to the transition from real to imaginary among the associated eigenvalues of the Hamiltonian, as depicted in Fig. 3. In the following, we will investigate how the boundary states change during $\mathcal{PT}$ symmetry breaking.

C. Robustness of edge states against random disorders

According to the bulk-boundary correspondence in the non-Abelian situation [4], the boundary states emerge in the finite system. In this section, we introduce the random disorder to study the robustness of these boundary states when the nonreciprocal hoppings are introduced in a finite system with 21 unit cells shown in Fig. 1. The random disorder is

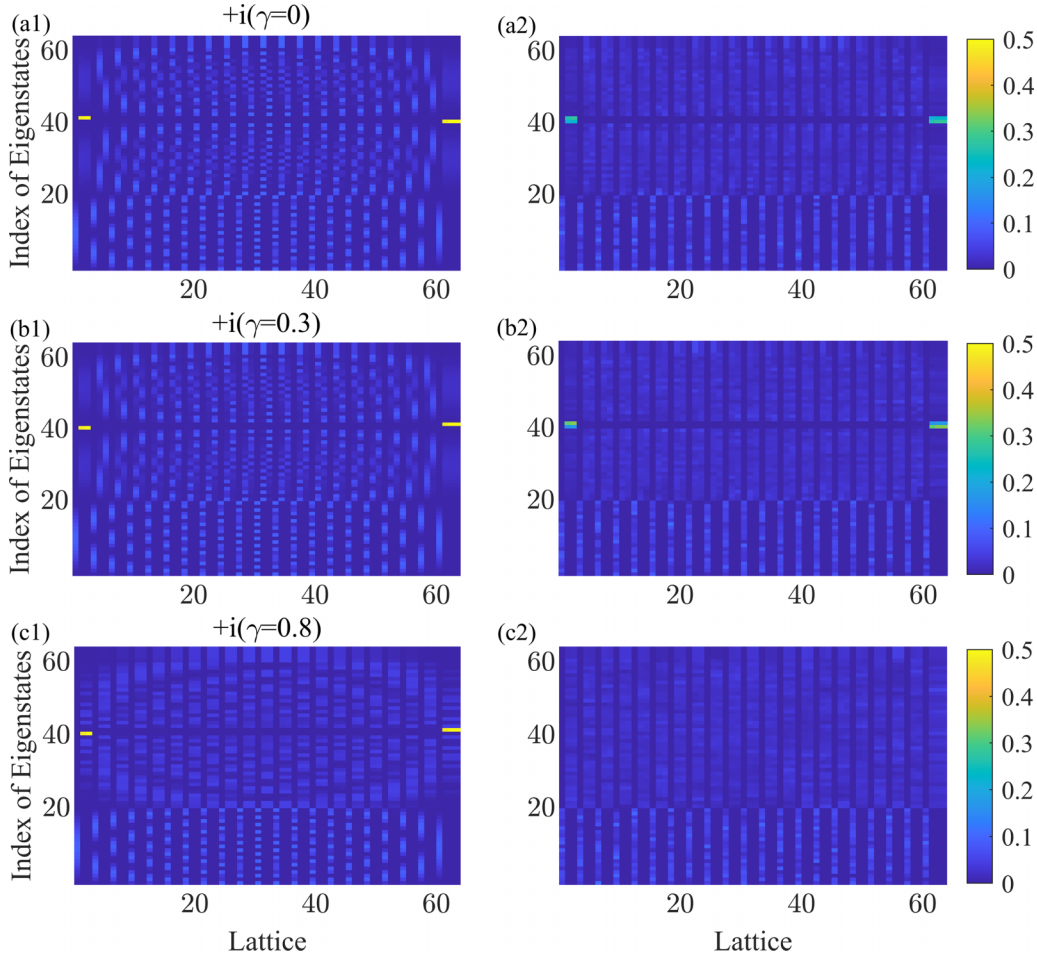

FIG. 5. The eigenstate distributions with different nonreciprocal hopping strengths (a1), (a2) $\gamma = 0$; (b1), (b2) $\gamma = 0.3$; and (c1), (c2) $\gamma = 0.8$ for topological charge $+i$. (a1)–(c1) The clean system without disorder. (a2)–(c2) The system with disorder strength $\delta = 0.3$. A slight modulation (1%) is applied to v_{XX} $(X = A, B, C)$ to avoid flat band. The edge states for $+i$, localized at the hard boundaries, are represented by yellow and cyan dots. Color bar represents the value of $|\psi|^2$. Here 21 unit cells are used in the numerical calculation; 100 configurations are calculated for disorder strength $\delta = 0.3$.

added to the on-site energy parameters: s_{AA}, s_{BB}, and s_{CC}, i.e., $s_{AAn} = s_{AA} + \delta\epsilon_n$, where n is the cell number, ϵ_n is uniformly distributed between -0.5 and 0.5, and δ denotes the disorder strength.

First, we compute 10 configurations for each disorder strength δ to observe the energy spectra. The numerical results for topological charges $+i$ and $+j$ are presented in Fig. 4. In a finite system, the boundary states appear in the second and first band gaps for the $+i$ and $+j$ cases, respectively, as expected. As illustrated in Figs. 4(a1) and 4(a2), the edge states remain robust against random disorder as long as both band gaps are not closed by the disorder when $\gamma = 0$. Once γ becomes nonzero, the energies of edge states acquire the imaginary parts $\pm\gamma$. Even as the disorder strength increases, the edge states remain robust until the $\mathcal{PT}$ symmetry is broken. We can observe that the edge states of topological charge $+i$ are robust against disorder and always stably located in the second band gap when $|\gamma| < 0.5$. For the topological charge $+j$ case, its edge states are robust against disorder when $|\gamma| < 1$. As an illustration, Figs. 4(b1) and 4(b2) show the energy spectra against the disorder strength when $\gamma = 0.3$ in the $+i$ case and $\gamma = 0.5$ in the $+j$ case. Once γ reaches the critical value for $\mathcal{PT}$ symmetry breaking, the band gaps close, and the edge state becomes embedded in the bulk states, as depicted in Figs. 4(c1) and 4(c2). For both the $+k$ and -1 cases, we observe that the edge states emerge and remain isolated when the $\mathcal{PT}$ symmetry is preserved, specifically when $|\gamma| < 0.5$. This prompts the question of whether these edge states remain robust in the presence of random disorder, especially in situations where the $\mathcal{PT}$ symmetry is broken.

We further investigate the eigenstate distributions for the topological charges $+i$ and $+j$ to confirm the robustness of edge states. Figures 5(a1)–5(c1) illustrate the eigenstate distributions of topological charge $+i$ with varying nonreciprocal hopping strengths γ in the clean system. It is evident that edge states consistently appear as nonreciprocal hopping strength γ reaches the critical value of 0.5, signifying that the second band gap is nontrivial. Figures 5(a2)–5(c2) display the eigenstate distributions for the disorder strength $\delta = 0.3$, keeping all other parameters the same as in Figs. 5(a1)–5(c1). Interestingly, the edge states vanish when $\gamma > 0.5$. Notably, in the non-Hermitian system, the edge states show resilience against disorder when the $\mathcal{PT}$ symmetry is unbroken, that is, $|\gamma| < 0.5$.

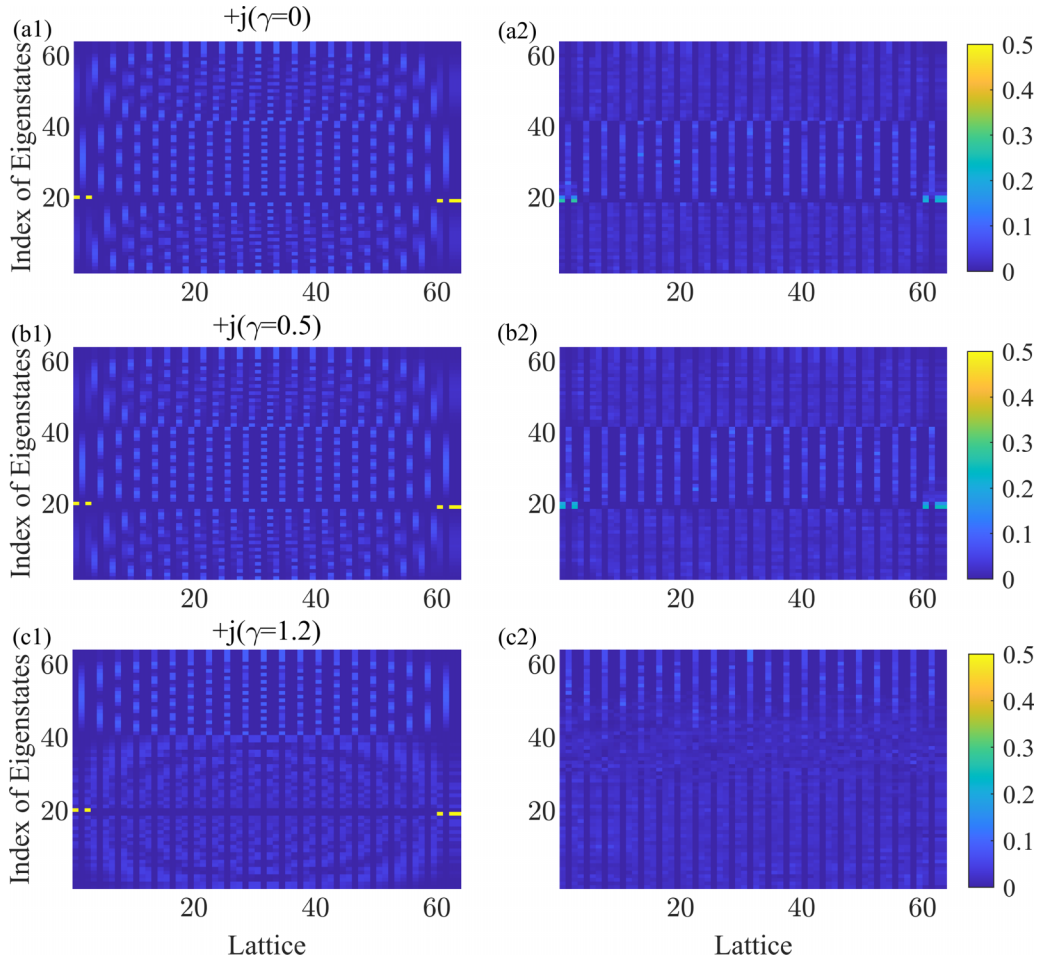

FIG. 6. The eigenstate distributions with different nonreciprocal hopping strengths (a1), (a2) $\gamma = 0$; (b1), (b2) $\gamma = 0.5$; and (c1), (c2) $\gamma = 1.2$ for topological charge $+j$. (a1)–(c1) The clean system without disorder. (a2)–(c2) The system with disorder strength $\delta = 0.3$. A slight modulation (1%) is applied to v_{XX} $(X = A, B, C)$ to avoid flat band. The edge states for $+j$, localized at the hard boundaries, are represented by yellow and cyan dots. Color bar represents the value of $|\psi|^2$. Here 21 unit cells are used in the numerical calculation; 100 configurations are calculated for disorder strength $\delta = 0.3$. Here $s_{BB} = 2.2$; other parameters are the same as those in Table I.

As we increase the nonreciprocal hopping strength γ in a clean system without the disorder, we consistently find that the edge states of $+j$ emerge. This indicates the first band gap is nontrivial, as shown in Fig. 6. These edge states remain robust against disorder, provided that they are protected by $\mathcal{PT}$ symmetry, specifically when $|\gamma| < 1$. In the clean system without the disorder, the edge states of the $+k$ and -1 cases consistently appear stable when nonreciprocal hopping strength $|\gamma| < 0.5$. This is consistent with the bulk energy value analysis in the previous section. In our study, there is no skin effect found.

D. Non-Hermitian non-Abelian domain wall states

According to the non-Abelian quotient relation in the Hermitian case [4], domain wall states can emerge when two subsystems carrying different topological charges are connected. This is indicated by $\Delta Q = Q_L/Q_R$ $(Q_{L,R}, \Delta Q \in \mathbb{Q})$. Here, we explore the situation where the subsystem becomes non-Hermitian. There are two different scenarios. First, domain wall states can arise when a Hermitian non-Abelian subsystem and a non-Hermitian non-Abelian subsystem carrying different topological charges are interconnected. Second, two non-Hermitian non-Abelian systems carrying different topological charges can be connected.

As an illustration, we numerically calculate the finite systems with topological charge pairs of $(+j, +k)$ and $(+j, +i)$, using different nonreciprocal hopping strengths $\gamma = 0.3$ and $\gamma = 0.8$. The results are shown in Fig. 7 and Fig. 8. The non-Abelian quotient relation prompts the emergence of a domain wall state, indicated by the topological charge i, in the second band gap region. Figure 7 confirms that a domain wall state appears regardless of which subsystem is non-Hermitian or even if both are non-Hermitian. These domain wall states show minor distribution differences in all cases. Furthermore, the domain wall state also appears when nonreciprocal hopping strength $\gamma = 0.8$ is introduced to the subsystem with topological charge $+k$, as shown in Figs. 7(a2) and 7(c2). In the $(+j, +i)$ system, the domain wall state, indicated by the topological charge k, emerges in the first band gap region as shown in Fig. 8 in different combinations. As demonstrated in Figs. 8(a2) and 8(c2), the domain wall state occurs when the nonreciprocal hopping strength of the introduced subsystem with topological charge $+i$ exceeds the $\mathcal{PT}$-symmetry-broken

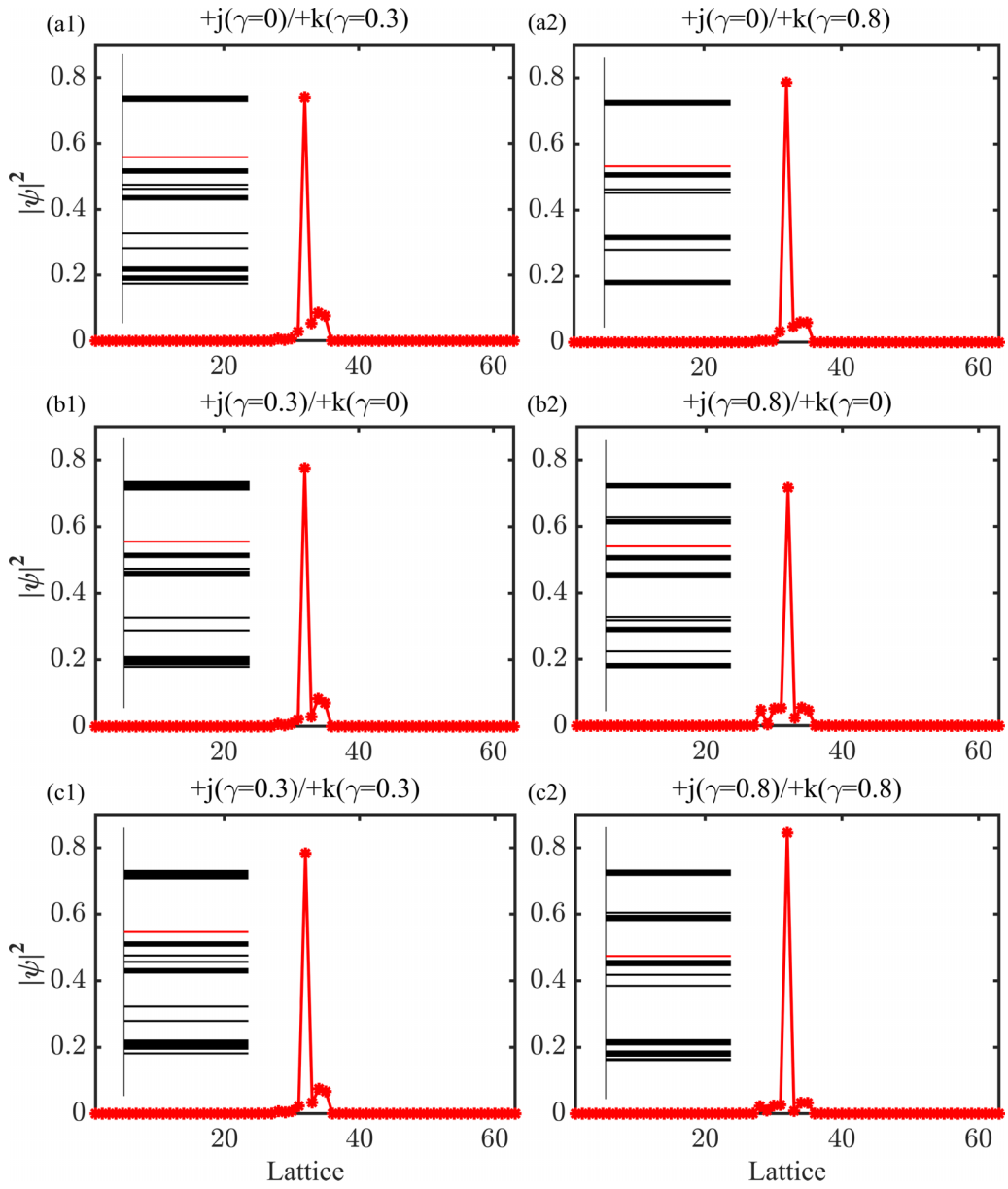

FIG. 7. Domain wall states corresponding to the topological charge pair of $(+j, +k)$ with varying nonreciprocal hopping strengths $\gamma = 0.3$ and $\gamma = 0.8$ in different subsystems. Here $s_{BB} = 2.2$ for charge $+j$; other parameters are the same as those in Table I. Each panel's inset shows the corresponding real part of energy spectrum, with the red line denoting the domain wall state. Here 21 unit cells are used.

value, $\gamma = 0.5$. We also discover that the domain wall state can emerge in systems that combine different topological charges.

Finally, we examine the robustness of the domain wall states when random disorder is introduced into the system. For example, we calculate the wave function distribution of the domain wall state in a random configuration with topological charge pairs of $(+j, +k)$. From Figs. 9(a1)–9(c1), we find that the domain wall states are robust against random disorder when $\gamma = 0.3$. However, when the nonreciprocal hopping strength $\gamma = 0.8$, the domain wall state persists only when it is added in the $+j$ subsystem, as shown in Fig. 9(b2). This is because the critical value of $\mathcal{PT}$ symmetry breaking for $+j$ is $\gamma = 1$, as we discussed previously. In the other two cases with $\gamma = 0.8$ in the $+k$ subsystem presented in Figs. 9(a2) and 9(c2), the domain wall states are not robust against random disorder and are no longer localized, since the $\mathcal{PT}$ symmetry is broken in the $+k$ region. For all other cases, we verify that the domain wall states are robust when the $\mathcal{PT}$ symmetry is maintained in the non-Hermitian case. Once the $\mathcal{PT}$ symmetry is broken, the domain wall states are no longer stable and can be disrupted by random perturbations.

IV. CONCLUSION

In summary, we have explicitly studied a non-Hermitian non-Abelian three-band tight-binding model by introducing nonreciprocal hopping. We discovered that the system's $\mathcal{PT}$ symmetry is broken as the nonreciprocal hopping strength increases up to a critical value. Note that the critical

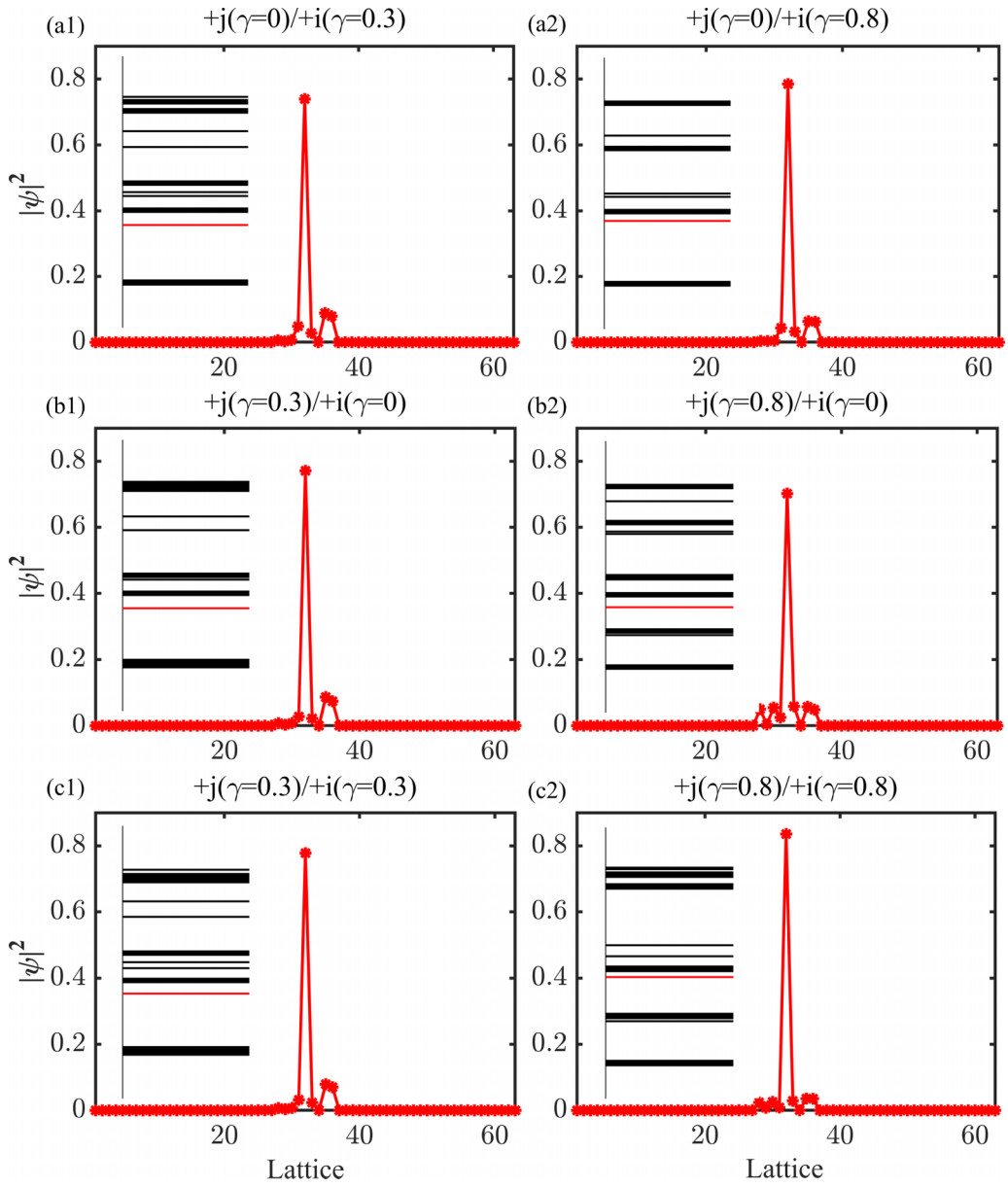

FIG. 8. Domain wall states corresponding to the topological charge pair of $(+j, +i)$ with different nonreciprocal hopping strengths $\gamma = 0.3$ and $\gamma = 0.8$ in different subsystems. Here $s_{BB} = 1.8$ for charge $+j$; other parameters are the same as those in Table I. Each panel's inset shows the corresponding real part of energy spectrum, with the red line denoting the domain wall state. Here 21 unit cells are used.

hopping values of $\mathcal{PT}$ transitions for the $\pm j$ case are different from other cases. The non-Hermitian non-Abelian topological charges and $\mathcal{PT}$ transition can be analytically described by the BWZ phase matrix. In the corresponding finite system, edge states emerge. Before the $\mathcal{PT}$ symmetry is broken, these states are stably localized at the system's two boundaries. However, after the symmetry is broken, the edge states become unstable and lose their robustness against disorder. We also examined the non-Abelian quotient relation in the non-Hermitian situation by investigating domain wall states between two subsystems carrying different non-Abelian topological charges. When two subsystems are protected by $\mathcal{PT}$ symmetry, the domain wall state remains stable and is robust against disorder. However, once either region's $\mathcal{PT}$ symmetry is broken, the domain wall state becomes unstable and loses its robustness against disorder. Our work provides valuable information for designing non-Hermitian non-Abelian systems with $\mathcal{PT}$ symmetry.

ACKNOWLEDGMENTS

We gratefully acknowledge support from the National Key R&D Program of China under Grant No. 2022YFA1404003, the National Natural Science Foundation of China (Grants No. 12074230, No. 12174231, and No. 12074190), the Fund for Shanxi "1331 Project", the Fundamental Research Program of Shanxi Province through Grant No. 202103021222001, and the Research Project Supported by the Shanxi Scholarship Council of China. This research was partially conducted using the High Performance Computer of Shanxi University.

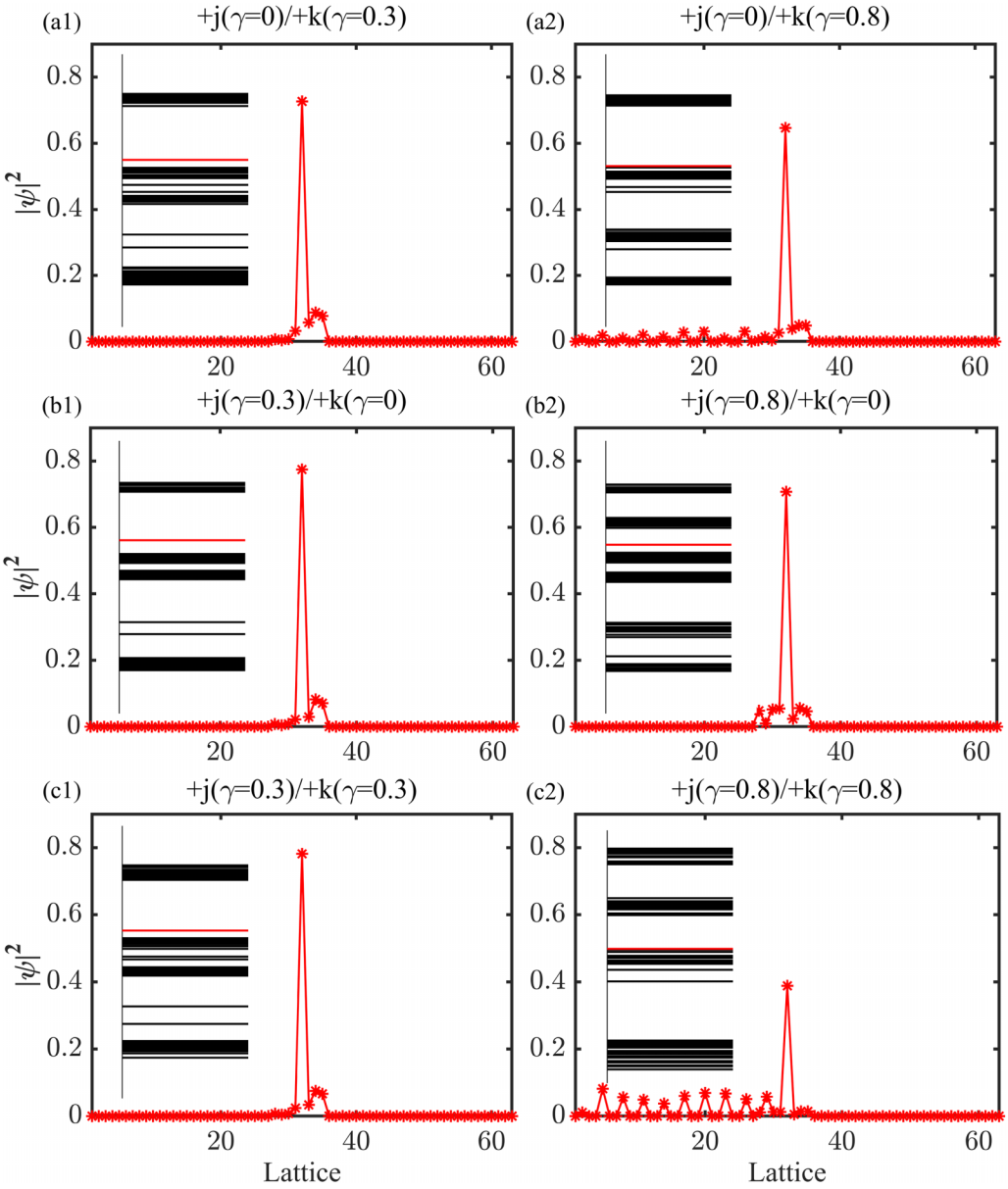

FIG. 9. Domain wall states corresponding to those in Fig. 7 in a random configuration with disorder strength $\delta = 0.13$. Other parameters are the same as those in Fig. 7.

APPENDIX: EIGEN-WAVE-FUNCTIONS FOR OTHER CASES

For $Q = +j, +k, -1$, the eigen-wave-functions can also be analytically solved as

$$\left|\psi_2^{(+j)}\right\rangle = \{0, 1, 0\}, \tag{A1}$$

$$\left|\psi_{1,3}^{(+j)}\right\rangle = \{-(\cos k \mp \sqrt{1-\gamma^2})/(\sin k + \gamma), 0, 1\}, \tag{A2}$$

$$\left|\phi_2^{(+j)}\right\rangle = \{0, 1, 0\}, \tag{A3}$$

$$\left|\phi_{1,3}^{(+j)}\right\rangle = \{-(\cos k \mp \sqrt{1-\gamma^2})/(\sin k - \gamma), 0, 1\}. \tag{A4}$$

$$\left|\psi_3^{(+k)}\right\rangle = \{0, 0, 1\}, \tag{A5}$$

$$\left|\psi_{1,2}^{(+k)}\right\rangle = \{(\cos k \mp \sqrt{1-4\gamma^2})/(\sin k - 2\gamma), 1, 0\}, \tag{A6}$$

$$\left|\phi_3^{(+k)}\right\rangle = \{0, 0, 1\}, \tag{A7}$$

$$\left|\phi_{1,2}^{(+k)}\right\rangle = \{(\cos k \mp \sqrt{1-4\gamma^2})/(\sin k + 2\gamma), 1, 0\}. \tag{A8}$$

$$\left|\psi_3^{(-1)}\right\rangle = \{0, 0, 1\}, \tag{A9}$$

$$\left|\psi_{1,2}^{(-1)}\right\rangle = \{(\cos 2k \pm \sqrt{1-4\gamma^2})/(\sin 2k + 2\gamma), 1, 0\}, \tag{A10}$$

$$\left|\phi_3^{(-1)}\right\rangle = \{0, 0, 1\}, \tag{A11}$$

$$\left|\phi_{1,2}^{(-1)}\right\rangle = \{(\cos 2k \pm \sqrt{1-4\gamma^2})/(\sin 2k - 2\gamma), 1, 0\}. \tag{A12}$$

Using these analytical expressions, we can derive the BWZ phase matrix in Eq. (23).

[1] Q. Wu, A. A. Soluyanov, and T. Bzdušek, Non-Abelian band topology in noninteracting metals, Science **365**, 1273 (2019).

[2] E. Yang, B. Yang, O. You, H.-C. Chan, P. Mao, Q. Guo, S. Ma, L. Xia, D. Fan, Y. Xiang, and S. Zhang, Observation of non-Abelian nodal links in photonics, Phys. Rev. Lett. **125**, 033901 (2020).

[3] A. Tiwari and T. Bzdušek, Non-Abelian topology of nodal-line rings in $\mathcal{PT}$-symmetric systems, Phys. Rev. B **101**, 195130 (2020).

[4] Q. Guo, T. Jiang, R.-Y. Zhang, L. Zhang, Z.-Q. Zhang, B. Yang, S. Zhang, and C. T. Chan, Experimental observation of non-Abelian topological charges and edge states, Nature (London) **594**, 195 (2021).

[5] M. Ezawa, Non-Hermitian non-Abelian topological insulators with $\mathcal{PT}$ symmetry, Phys. Rev. Res. **3**, 043006 (2021).

[6] P. M. Lenggenhager, X. Liu, S. S. Tsirkin, T. Neupert, and T. Bzdušek, From triple-point materials to multiband nodal links, Phys. Rev. B **103**, L121101 (2021).

[7] T. Jiang, R.-Y. Zhang, Q. Guo, B. Yang, and C. T. Chan, Two-dimensional non-Abelian topological insulators and the corresponding edge/corner states from an eigenvector frame rotation perspective, Phys. Rev. B **106**, 235428 (2022).

[8] T. Li and H. Hu, Floquet non-Abelian topological insulator and multifold bulk-edge correspondence, Nat. Commun. **14**, 6418 (2023).

[9] D. Wang, B. Yang, Q. Guo, R.-Y. Zhang, L. Xia, X. Su, W.-J. Chen, J. Han, S. Zhang, and C. T. Chan, Intrinsic in-plane nodal chain and generalized quaternion charge protected nodal link in photonics, Light Sci. Appl. **10**, 83 (2021).

[10] B. Jiang, A. Bouhon, Z.-K. Lin, X. Zhou, B. Hou, F. Li, R.-J. Slager, and J.-H. Jiang, Experimental observation of non-Abelian topological acoustic semimetals and their phase transitions, Nat. Phys. **17**, 1239 (2021).

[11] B. Peng, A. Bouhon, B. Monserrat, and R.-J. Slager, Phonons as a platform for non-Abelian braiding and its manifestation in layered silicates, Nat. Commun. **13**, 423 (2022).

[12] T. Jiang, Q. Guo, R.-Y. Zhang, Z.-Q. Zhang, B. Yang, and C. T. Chan, Four-band non-Abelian topological insulator and its experimental realization, Nat. Commun. **12**, 6471 (2021).

[13] M. Wang, S. Liu, Q. Ma, R.-Y. Zhang, D. Wang, Q. Guo, B. Yang, M. Ke, Z. Liu, and C. T. Chan, Experimental observation of non-Abelian earring nodal links in phononic crystals, Phys. Rev. Lett. **128**, 246601 (2022).

[14] Z. Gong, Y. Ashida, K. Kawabata, K. Takasan, S. Higashikawa, and M. Ueda, Topological phases of non-Hermitian systems, Phys. Rev. X **8**, 031079 (2018).

[15] E. J. Bergholtz, J. C. Budich, and F. K. Kunst, Exceptional topology of non-Hermitian systems, Rev. Mod. Phys. **93**, 015005 (2021).

[16] K. Kawabata, K. Shiozaki, M. Ueda, and M. Sato, Symmetry and topology in non-Hermitian physics, Phys. Rev. X **9**, 041015 (2019).

[17] D. S. Borgnia, A. J. Kruchkov, and R.-J. Slager, Non-Hermitian boundary modes and topology, Phys. Rev. Lett. **124**, 056802 (2020).

[18] C. M. Bender and S. Boettcher, Real spectra in non-Hermitian Hamiltonians having $\mathcal{PT}$ symmetry, Phys. Rev. Lett. **80**, 5243 (1998).

[19] S. Malzard, C. Poli, and H. Schomerus, Topologically protected defect states in open photonic systems with non-Hermitian charge-conjugation and parity-time symmetry, Phys. Rev. Lett. **115**, 200402 (2015).

[20] Y. Ashida, Z. Gong, and M. Ueda, Non-Hermitian physics, Adv. Phys. **69**, 249 (2020).

[21] H. Jiang, C. Yang, and S. Chen, Topological invariants and phase diagrams for one-dimensional two-band non-Hermitian systems without chiral symmetry, Phys. Rev. A **98**, 052116 (2018).

[22] S. Yao and Z. Wang, Edge states and topological invariants of non-Hermitian systems, Phys. Rev. Lett. **121**, 086803 (2018).

[23] L. Li, C. H. Lee, and J. Gong, Impurity induced scale-free localization, Commun. Phys. **4**, 42 (2021).

[24] F. Roccati, Non-Hermitian skin effect as an impurity problem, Phys. Rev. A **104**, 022215 (2021).

[25] N. Okuma and M. Sato, Non-Hermitian topological phenomena: A review, Annu. Rev. Condens. Matter Phys. **14**, 83 (2023).

[26] S. Liu, R. Shao, S. Ma, L. Zhang, O. You, H. Wu, Y. J. Xiang, T. J. Cui, and S. Zhang, Non-Hermitian skin effect in a non-Hermitian electrical circuit, Research **2021**, 5608038 (2021).

[27] F. Song, S. Yao, and Z. Wang, Non-Hermitian skin effect and chiral damping in open quantum systems, Phys. Rev. Lett. **123**, 170401 (2019).

[28] Y. Cao, Y. Li, and X. Yang, Non-Hermitian bulk-boundary correspondence in a periodically driven system, Phys. Rev. B **103**, 075126 (2021).

[29] L. Xiao, T. Deng, K. Wang, G. Zhu, Z. Wang, W. Yi, and P. Xue, Non-Hermitian bulk-boundary correspondence in quantum dynamics, Nat. Phys. **16**, 761 (2020).

[30] R. Koch and J. C. Budich, Bulk-boundary correspondence in non-Hermitian systems: Stability analysis for generalized boundary conditions, Eur. Phys. J. D **74**, 70 (2020).

[31] L. Jin and Z. Song, Bulk-boundary correspondence in a non-Hermitian system in one dimension with chiral inversion symmetry, Phys. Rev. B **99**, 081103(R) (2019).

[32] E. Edvardsson, F. K. Kunst, and E. J. Bergholtz, Non-Hermitian extensions of higher-order topological phases and their biorthogonal bulk-boundary correspondence, Phys. Rev. B **99**, 081302(R) (2019).

[33] F. K. Kunst, E. Edvardsson, J. C. Budich, and E. J. Bergholtz, Biorthogonal bulk-boundary correspondence in non-Hermitian systems, Phys. Rev. Lett. **121**, 026808 (2018).

[34] K. Kawabata, T. Bessho, and M. Sato, Classification of exceptional points and non-Hermitian topological semimetals, Phys. Rev. Lett. **123**, 066405 (2019).

[35] Ş. K. Özdemir, S. Rotter, F. Nori, and L. Yang, Parity-time symmetry and exceptional points in photonics, Nat. Mater. **18**, 783 (2019).

[36] M.-A. Miri and A. Alù, Exceptional points in optics and photonics, Science **363**, eaar7709 (2019).

[37] W. Hu, H. Wang, P. P. Shum, and Y. D. Chong, Exceptional points in a non-Hermitian topological pump, Phys. Rev. B **95**, 184306 (2017).

[38] F. Minganti, A. Miranowicz, R. W. Chhajlany, and F. Nori, Quantum exceptional points of non-Hermitian Hamiltonians and Liouvillians: The effects of quantum jumps, Phys. Rev. A **100**, 062131 (2019).

[39] Y. Xu, S.-T. Wang, and L.-M. Duan, Weyl exceptional rings in a three-dimensional dissipative cold atomic gas, Phys. Rev. Lett. **118**, 045701 (2017).

[40] R. El-Ganainy, K. G. Makris, M. Khajavikhan, Z. H. Musslimani, S. Rotter, and D. N. Christodoulides, Non-Hermitian physics and $\mathcal{PT}$ symmetry, Nat. Phys. **14**, 11 (2018).

[41] S. Weimann, M. Kremer, Y. Plotnik, Y. Lumer, S. Nolte, K. G. Makris, M. Segev, M. C. Rechtsman, and A. Szameit, Topologically protected bound states in photonic parity-time-symmetric crystals, Nat. Mater. **16**, 433 (2017).

[42] A. I. Nesterov and F. A. de la Cruz, Complex magnetic monopoles, geometric phases and quantum evolution in the vicinity of diabolic and exceptional points, J. Phys. A: Math. Theor. **41**, 485304 (2008).

[43] U. Günther, I. Rotter, and B. F. Samsonov, Projective Hilbert space structures at exceptional points, J. Phys. A: Math. Theor. **40**, 8815 (2007).

[44] Y. Huang and B. I. Shklovskii, Anderson transition in three-dimensional systems with non-Hermitian disorder, Phys. Rev. B **101**, 014204 (2020).

[45] L. G. Molinari, Non-Hermitian spectra and Anderson localization, J. Phys. A: Math. Theor. **42**, 265204 (2009).

[46] Y. C. Hu and T. L. Hughes, Absence of topological insulator phases in non-Hermitian $\mathcal{PT}$-symmetric Hamiltonians, Phys. Rev. B **84**, 153101 (2011).

[47] I. Rotter, A non-Hermitian Hamilton operator and the physics of open quantum systems, J. Phys. A: Math. Theor. **42**, 153001 (2009).

[48] S. Longhi, Convective and absolute $\mathcal{PT}$-symmetry breaking in tight-binding lattices, Phys. Rev. A **88**, 052102 (2013).

[49] D. C. Brody, Biorthogonal quantum mechanics, J. Phys. A: Math. Theor. **47**, 035305 (2014).

[50] H. Hu and E. Zhao, Knots and non-Hermitian Bloch bands, Phys. Rev. Lett. **126**, 010401 (2021).